

Constrained Bimanual Planning with Analytic Inverse Kinematics

Thomas Cohn, Seiji Shaw, Max Simchowitz, and Russ Tedrake

Abstract—In order for a bimanual robot to manipulate an object that is held by both hands, it must construct motion plans such that the transformation between its end effectors remains fixed. This amounts to complicated nonlinear equality constraints in the configuration space, which are difficult for trajectory optimizers. In addition, the set of feasible configurations becomes a measure zero set, which presents a challenge to sampling-based motion planners. We leverage an analytic solution to the inverse kinematics problem to parametrize the configuration space, resulting in a lower-dimensional representation where the set of valid configurations has positive measure. We describe how to use this parametrization with existing algorithms for motion planning, including sampling-based approaches, trajectory optimizers, and techniques that plan through convex inner-approximations of collision-free space.

I. INTRODUCTION

Constrained bimanual planning presents a major challenge to traditional motion planning algorithms. When moving an object that is held by both hands, the robot must carefully move both arms in concert to ensure that the transformation between the end effectors remains constant. Such task space constraints appear as complicated nonlinear equalities in configuration space. In effect, the feasible set becomes measure zero, so samples must either be drawn directly from the constraint manifold or projected onto it. Furthermore, these implicit constraints do not have an obvious explicitization.

In the existing literature, there are general techniques for handling task-space constraints in configuration-space planning. Sampling-based planners can project samples onto the constraint manifold [1], or use numerical continuation [2] to construct piecewise-linear approximations. Constraints can also be relaxed [3] or enforced directly with trajectory optimization [4]. In the case of certain bimanual planning problems, there is additional structure that is not exploited by these general methods. For certain classes of robot arms, *analytic inverse kinematics* (analytic IK) can be used to map an end-effector pose (along with additional parameters to resolve kinematic redundancy) to joint angles in closed form. Such solutions are specific to certain classes of robot arms, but are a powerful tool to be leveraged if available. Fortunately, analytic IK is available for many popular robot arms available today, including the KUKA iiwa. See Figure 1.

This work was supported by Amazon.com, PO No. 2D-06310236, the MIT Quest for Intelligence, and the National Science Foundation Graduate Research Fellowship Program under Grant No. 2141064. Any opinions, findings, and conclusions or recommendations expressed in this material are those of the author(s) and do not necessarily reflect the views of the National Science Foundation. The authors are with the Computer Science and Artificial Intelligence Laboratory (CSAIL), Massachusetts Institute of Technology, Cambridge, Massachusetts [tcohn, seijis, msimchow, russt]@mit.edu

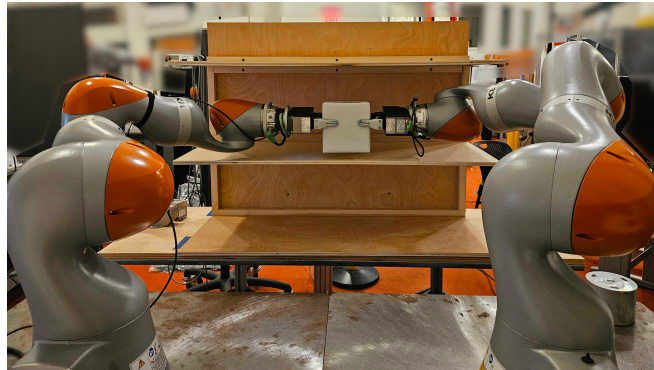


Fig. 1: Hardware setup for our experiments. The two KUKA iiwa arms must work together to move an objects between the shelves, avoiding collisions and respecting the kinematic constraint.

If a robot must move an object that it is holding with both hands, we propose constructing a plan for one “controllable” arm, and then the other “subordinate” arm can be made to follow it via an analytic IK mapping. Configurations where the subordinate arm cannot reach the end-effector of the primary arm, or where doing so would require violating joint limits, are treated as obstacles. In this way, we parametrize the constraint manifold, so that the feasible set has positive measure in the new planning space. This enables most standard motion planning algorithms to be applied with only slight modifications.

The remainder of this paper is organized as follows. First, we give an overview of the existing techniques used for constrained motion planning, and describe the available analytic IK solutions. Then, we present our parametrization of the constraint manifold for bimanual planning, and discuss its relevant geometric and topological properties. We describe the slight modifications which are necessary to adapt standard planning algorithms (including sampling-based planning and trajectory optimization) to operate in this framework. We then present a technique for generating convex sets in this new configuration space, such that every configuration within such a set is collision free and kinematically valid. These sets are essential for planning frameworks such as the Graph of Convex Sets (GCS) [5]. Finally, we present various experiments demonstrating the efficacy of these new techniques.

II. RELATED WORK

Motion planning with task constraints is a well-studied problem in robotics. Techniques for sampling-based planning

can broadly be categorized by their methodologies:

- Relax the constraints (with real or simulated compliance) to give the feasible set nonzero volume [3], [6].
- Project samples to the constraint manifold [1], [7], [8].
- Construct piecewise-linear approximations of the constraint manifold [9], [10], [11], [12].
- Parametrize of the constraint manifold to eliminate constraints [13], [14].
- Build offline approximations of the constraint manifold, to simplify online planning [15], [16].

See the survey paper [17] for an overview of these methods.

Beyond sampling-based planning, standard nonconvex trajectory optimization approaches can handle arbitrary constraints, although they will generally only converge to a feasible solution with good initialization [17]. [4] performed nonconvex trajectory optimization on manifolds.

Inverse kinematics (IK) – computing robot joint angles so as to place the end effector at a given configuration – is a powerful tool for handling certain kinematic constraints. IK can be leveraged to find stable, collision-free configurations for a humanoid robot, towards whole-body planning [18], to help a robot arm follow a prescribed task-space trajectory [19], and to satisfy the kinematic constraints that arise when manipulating articulated objects [20]. Differential IK techniques can be used to follow task space trajectories, while satisfying constraints [21, §10.3], [22, §3.10].

A key part of our work is to use IK to parametrize the constraint manifold, thus eliminating the nonlinear equality constraints. IK solutions are often computed by solving a nonconvex mathematical program. The tools of algebraic geometry can be used to reformulate certain IK problems as systems of polynomial equations, which can be solved as eigenvalue problems [23], [24], [25]. While simpler than a nonconvex optimization problem, we require a closed-form solution for our desired parametrization. For robot arms with six revolute joints with certain kinematic structure, closed-form geometric solutions can be found by dividing the joints into two sets of three joints, and treating each of these as “virtual” spherical joints [26, §2.12]. IKFast [27] can be used to automatically construct analytic IK solutions for broad classes of robot arm kinematics, and is available as part of the OpenRAVE toolkit [28]. Some arms have geometric solutions, such as the Universal Robotics UR-5/UR-10 [29].

Robot arms with more than six degrees of freedom have kinematic redundancy – the arm can be moved while keeping its end effector fixed. This is called *self-motion* and is useful for avoiding obstacles and joint limits, but implies the kinematic mapping cannot be bijective. [30] avoids this problem by computing a globally-consistent pseudoinverse, but this discards the redundancy, artificially restricting the configuration space. Other approaches characterize the redundancy as an additional parameter to be controlled in addition to the end-effector pose. [31] presents a strategy for treating specific joints in a 7DoF arm as free parameters, reducing the problem to that of a 6DoF arm with a structure amenable to a closed-form solution. IKFast can discretize any additional joints. Similar to the sphere-sphere 6DoF arms,

certain 7DoF arms have a sphere-revolute-sphere kinematic structure, leading to elegant geometric solutions [32], [33]. Specific geometric solutions are available for many common robot arms, including the KUKA iiwa [34], Franka Emika Panda [35], and the Barrett WAM [36].

Our parametrization can be combined with many planning algorithms to form a complete system. In this paper, we specifically examine the canonical sampling-based planners: Rapidly-Exploring Random Trees (RRTs) [37] and Probabilistic Roadmaps (PRMs) [38]. Our contributions can also be used with the many extensions to these techniques [39], [40], [41], [42], [43], [44], [45]. We also describe how to use standard kinematic trajectory optimization techniques [22, §7.2], [46], [47], [48]. Finally, we describe how to extend the IRIS-NP algorithm [49] for computing convex collision-free sets to use our parametrization of the configuration space; such sets can be planned across with the GCS planning framework [5]. (These sets can also be used with other “convex set planning algorithms” [50], [51], [52].)

III. METHODOLOGY

We introduce a bijective mapping between joint angles and end-effector pose for a single arm with analytic IK. We then use this mapping to parametrize the set of valid configurations for constrained bimanual manipulation. The joint angles of one arm are treated as free variables for the parametrized configuration space, and the aforementioned mapping is used to determine the joint angles for the other arm. Finally, we explain the modifications needed to adapt existing planning algorithms to utilize this parametrization.

A. Topology of Inverse Kinematics

The topological and geometric properties of inverse kinematic mappings are a classic area of study in robotics [53], [54], [55]. For an arm with $n \geq 6$ revolute joints, the configuration space is $\mathcal{C} \subseteq \mathbb{T}^n$, where \mathbb{T}^n denotes the n -torus. The forward kinematic mapping $f : \mathcal{C} \rightarrow \text{SE}(3)$ computes the end-effector pose of the arm for a given choice of each joint angle. We define the reachable set $\mathcal{X} = \{f(\theta) : \theta \in \mathcal{C}\} \subseteq \text{SE}(3)$. To construct a homeomorphism between subsets of \mathcal{C} and \mathcal{X} , we must restrict our domain of attention to avoid singular configurations, and augment \mathcal{X} with additional degrees of freedom to match dimensions.

We give an overview of the terminology introduced in [54] for describing the global behavior of inverse kinematic mappings. A configuration for which the Jacobian of f is full-rank is called a *regular point*; otherwise, it is called a *critical point*. Because f is not injective, the preimage of a single end-effector pose may contain only critical points, only regular points, or some of both; it is respectively called a *critical value*, *regular value*, and *coregular value*. \mathcal{W} -sheets are the connected components of regular values in \mathcal{X} whose boundaries are the coregular values of f . The connected components of the preimages of \mathcal{W} -sheets are called \mathcal{C} -bundles and form a partition the regular points of \mathcal{C} . For

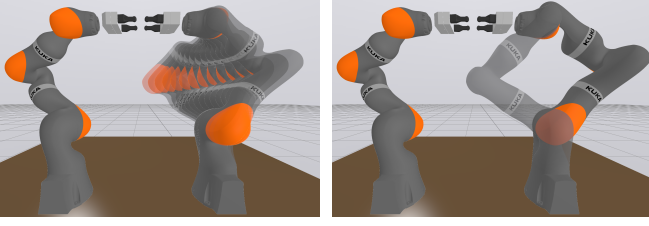


Fig. 2: Continuous (left) and discrete (right) self motions of a 7DoF arm.

a regular value $x \in \mathcal{X}$, we have

$$f^{-1}(x) = \bigcup_{i=1}^m \mathcal{M}_i(x), \quad (1)$$

where the $\mathcal{M}_i(x)$ are *self-motion manifolds* of x , so called because motion within them does not affect the end-effector pose. The label i is called the *global configuration parameter*, and a choice of $\psi \in \mathcal{M}_i(x)$ is called the *redundancy parameter*. For robot arms in 3D space, the number of self-motion manifolds is at most 16; within a \mathcal{C} -bundle, the self-motion manifolds are homotopic; and if the arm has only revolute joints, then the self-motion manifolds are diffeomorphic to \mathbb{T}^{n-6} [54]. (If $n = 6$, then the \mathcal{M}_i are zero-dimensional, i.e., discrete points.) Examples of the continuous and discrete self motions for a 7DoF arm are shown in Figure 2.

The \mathcal{C} -bundle/ \mathcal{W} -sheet machinery allows us to construct well-defined IK mappings. Let $\mathcal{W}_j \subseteq \mathcal{X}$ be a \mathcal{W} -sheet, and let $x_0 \in \mathcal{W}_j$. Then there is a smooth injection $g_{i,j} : \mathcal{W}_j \times \mathcal{M}_i(x_0) \rightarrow \mathcal{C}$. Since the self-motion manifolds are homotopic within a \mathcal{C} -bundle, they are uniquely described in terms of their choice of \mathcal{C} -bundle and \mathcal{W} -sheet, so we use the shorthand $\mathcal{M}_{i,j}$ in place of $\mathcal{M}_i(x_0)$. If we let $h_{i,j}$ map joint angles to their corresponding redundancy parameter, then $(f, h_{i,j}) \circ g_{i,j}$ is the identity mapping on $\mathcal{W}_j \times \mathcal{M}_{i,j}$. Thus, with appropriate restrictions in domain and range, we have a bijection between the arm’s joint angles and the product of its end-effector pose and redundancy parameters. The set $\mathcal{C}_{i,j}$, defined as the image of $g_{i,j}$, is the set of joint angles which can be handled by these mappings.

B. Parametrizing the Kinematically Constrained Space

Now, we turn our attention to the bimanual case. We use an additional subscript to denote which arm the sets and maps correspond to; for example, \mathcal{X}_L is the reachable set of the “left” arm, and $g_{i,j,R}$ denotes the inverse kinematic mapping for the “right” arm.

When a rigid object is held with both end effectors, a rigid transformation $\mathcal{T} \in \text{SE}(3)$ between them becomes fixed; we let $\phi_{\mathcal{T}} : \mathcal{X}_L \rightarrow \text{SE}(3)$ take in an end-effector pose for the left arm (henceforth called the *controlled arm*), and output the target end-effector pose for the right arm (henceforth called the *subordinate arm*). We let $\mathcal{X}_{\mathcal{T}} := \{(x, \phi_{\mathcal{T}}(x)) : x \in \mathcal{X}_L\} \subset \mathcal{X}_L \times \text{SE}(3)$ denote the space of end-effector poses which are feasible for the controlled arm and for which the pose of subordinate end-effector respects transformation

\mathcal{T} . Note that this latter pose may not be reachable for the subordinate arm, and a choice of redundancy parameter may require a violation of its joint limits. We treat both of these cases as abstract obstacles in the configuration space.

For the remainder of the paper, we fix the global configuration parameter i and choice of \mathcal{W} -sheet j for the second arm. Let \mathcal{T} be the desired end-effector transformation. We define a *parametrized* configuration space $\mathcal{Q} := \mathcal{C}_L \times \mathcal{M}_{i,j,R}$. $q \in \mathcal{Q}$ determines joint angles for both arms via the mapping

$$\xi : (\theta_L, \psi_R) \mapsto (\theta_L, g_{i,j,R}(\phi_{\mathcal{T}}(f_L(\theta_L)), \psi_R)). \quad (2)$$

For more details on why we select this specific parametrization, see Section V. Let θ_{\min} and θ_{\max} be the lower and upper joint limits. A configuration (θ_L, ψ_R) is valid if:

$$\phi_{\mathcal{T}}(f_L(\theta_L)) \in \mathcal{W}_{j,R} \quad (\text{Respect reachability.}) \quad (3a)$$

$$\theta_{\min} \leq \xi(\theta_L, \psi_R) \leq \theta_{\max} \quad (\text{Respect joint limits.}) \quad (3b)$$

We call the set of configurations satisfying these constraints $\mathcal{Q}_{\text{VALID}}$. For $q \in \mathcal{Q}$, if the robot is collision free for the joint angles $\xi(q)$, we say $q \in \mathcal{Q}_{\text{FREE}}$.

C. Reformulating the Motion Planning Problem

Let $\mathfrak{s}, \mathfrak{t} \in \mathcal{C}_L \times \mathcal{C}_R$ be the start and goal configurations. The *constrained motion planning problem* requires finding a path $\gamma = (\gamma_L, \gamma_R) : [0, 1] \rightarrow \mathcal{C}_L \times \mathcal{C}_R$ by solving:

$$\text{argmin } L(\gamma) \quad (4a)$$

$$\text{s.t. } \gamma(t) \text{ collision free} \quad \forall t \in [0, 1] \quad (4b)$$

$$\phi_{\mathcal{T}}(f_L(\gamma_L(t))) = f_R(\gamma_R(t)) \quad \forall t \in [0, 1] \quad (4c)$$

$$\gamma(0) = \mathfrak{s}, \gamma(1) = \mathfrak{t}. \quad (4d)$$

(L denotes the arc length functional, but can be replaced with another cost.) The main challenge this formulation presents is the nonlinear equality constraint (4c), as this requires γ lie along a measure-zero set. Trajectory optimizers may struggle with (4c), and sampling-based planners must use one of the techniques described in Section II.

Our *parametrized motion planning problem* is written in terms of a trajectory $\bar{\gamma} : [0, 1] \rightarrow \mathcal{Q}$, with start $\bar{\mathfrak{s}}$ and goal $\bar{\mathfrak{t}}$ satisfying $\xi(\bar{\mathfrak{s}}) = \mathfrak{s}$ and $\xi(\bar{\mathfrak{t}}) = \mathfrak{t}$:

$$\text{argmin } L(\xi \circ \bar{\gamma}) \quad (5a)$$

$$\text{s.t. } (\xi \circ \bar{\gamma})(t) \text{ collision free} \quad \forall t \in [0, 1] \quad (5b)$$

$$\bar{\gamma}(t) \in \mathcal{Q}_{\text{VALID}} \quad \forall t \in [0, 1] \quad (5c)$$

$$\bar{\gamma}(0) = \bar{\mathfrak{s}}, \bar{\gamma}(1) = \bar{\mathfrak{t}}. \quad (5d)$$

This formulation includes the implicit requirement that the entire planned trajectory be within a single \mathcal{C} -bundle, due to the restricted domain of ξ . In Section IV, we demonstrate that this theoretical limitation is not a major roadblock to our framework’s efficacy. A major advantage our parametrization (and parametrization methods in general) is that by construction, the end-effector poses $(f_L, f_R) \circ \xi(\bar{\gamma}(t))$ are *guaranteed* to be related by transformation \mathcal{T} . For other methodologies, the constraints are only satisfied at discrete points along the trajectory. (See Figure 3.)

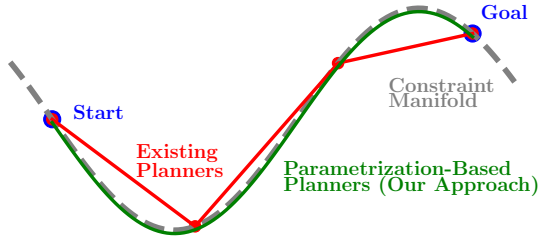


Fig. 3: Most existing planners can only enforce constraints at discrete points along the trajectory. Parametrization-based planners (including our approach) satisfy constraints at all points by construction.

D. Motion Planning with the Parametrization

Constraint (5c) is a nonlinear *inequality* constraint, so feasible trajectories are constrained to lie in a positive volume set $\mathcal{Q}_{\text{VALID}} \cap \mathcal{Q}_{\text{FREE}}$. This enables standard, unconstrained motion planning algorithms to function with only slight modifications.

1) *Sampling-Based Planning*: The changes required for sampling based planners can be summarized as treating points outside $\mathcal{Q}_{\text{VALID}}$ as being in collision. Because $\mathcal{Q}_{\text{VALID}} \cap \mathcal{Q}_{\text{FREE}}$ has positive measure, rejection sampling can be used to draw valid samples. When connecting samples (as in the “Extend” procedure of an RRT or “Connect” procedure of a PRM), the frequency with which collisions are checked must be adjusted, since distance in the parametrized space \mathcal{Q} differs from distance in the full configuration space $\mathcal{C}_{\text{L}} \times \mathcal{C}_{\text{R}}$. In particular, a small motion in \mathcal{Q} can lead to a relatively large motion in $\mathcal{C}_{\text{L}} \times \mathcal{C}_{\text{R}}$, so collision checking must be done more frequently (or at a varying scale).

2) *Trajectory Optimization*: Trajectory optimization in configuration space is already nonconvex, so implementing constraints (5b) and (5c) requires no algorithmic changes. As with sampling-based planning, collision avoidance (and other constraints applied to the full configuration space) must be enforced at a finer resolution.

3) *Graph of Convex Sets*: Let $\mathcal{U} \subseteq \mathcal{Q}_{\text{VALID}} \cap \mathcal{Q}_{\text{FREE}}$ be convex. Then the kinematic validity (and collision-free nature) of a linear path through \mathcal{U} is guaranteed if its endpoints are contained in \mathcal{U} . Thus, the Graph of Convex Sets Planner (GCS) can function as expected with two small modifications. We minimize the arc length in the parametrized space $L(\bar{\gamma})$, as this objective provides a useful convex surrogate for the true (nonconvex) objective (5a). Also, for robot arms composed of revolute joints, the self-motion parameters are angle-valued, so one can either make cuts to the configuration space and treat it as Euclidean, or use the extension *Graphs of Geodesically-Convex Sets* (GGCS) [56]. The product of the angle-valued self-motion parameters will be a circle or n-torus, both of which admit a flat metric [57, p.345]. If we plan across geodesically convex (g-convex) subsets of $\mathcal{Q}_{\text{VALID}} \cap \mathcal{Q}_{\text{FREE}}$, then the problem satisfies the sufficient conditions presented in Assumptions 1 and 2 of [56]. These assumptions guarantee that the resulting

Algorithm 1: Constrained IRIS (Single Iteration)

Input: Bounding Box $\mathcal{H}_0(A_0, b_0)$
Hyperellipsoid $\mathcal{E}(C, d)$ s.t. $d \in \mathcal{H}_0(A_0, b_0)$
Constraint Sets $\mathbf{CS}_1, \dots, \mathbf{CS}_k$
Output: Halfspace Intersection $\mathcal{H}(A, b)$

- 1 $A \leftarrow A_0, b \leftarrow b_0$
- 2 **for** $\mathbf{CS} = \mathbf{CS}_1, \dots, \mathbf{CS}_k$ **do**
- 3 **repeat**
- 4 $(a^*, b^*) \leftarrow \text{SOLVE}[(6), \{A, b, C, d, \mathbf{CS}\}]$
- 5 $A \leftarrow \text{VSTACK}(A, a^*), b \leftarrow \text{VSTACK}(b, b^*)$
- 6 **until** INFEASIBLE
- 7 **return** $\mathcal{H}(A, b)$

path will be kinematically valid and collision-free at all times.

E. Constructing Convex Valid Sets

To use (G)GCS, one must construct (g-)convex subsets of $\mathcal{Q}_{\text{VALID}} \cap \mathcal{Q}_{\text{FREE}}$. Our approach is based on the IRIS-NP algorithm [49], which uses a counterexample search to find configurations where the robot is in collision, and putting up hyperplanes to avoid such configurations. Given a hyperellipsoid $\mathcal{E}(C, d) = \{q : \|q - d\|_C^2 \leq 1\}$ (using the notation $\|q - d\|_C^2 = (q - d)^T C^T C (q - d)$), a halfspace intersection $\mathcal{H}(A, b) = \{q : Aq \leq b\}$, and a *constraint set* \mathbf{CS} , the *generalized counterexample search program* is

$$\min_q \|q - d\|_C^2 \quad (6a)$$

$$\text{s.t. } Aq \leq b \quad (6b)$$

$$q \notin \mathbf{CS}. \quad (6c)$$

Given a bounding box $\mathcal{H}_0(A_0, b_0)$, a hyperellipsoid $\mathcal{E}(C, d)$ with $d \in \mathcal{H}_0(A_0, b_0)$, and a list of configuration-space constraints $\mathbf{CS}_1, \dots, \mathbf{CS}_k$ to enforce, Algorithm 1 produces a halfspace intersection $\mathcal{H}(A, b) \subseteq \mathcal{H}_0(A_0, b_0)$ such that every point in $\mathcal{H}(A, b)$ satisfies the constraints.

We now describe the constraint sets \mathbf{CS} needed for Algorithm 1 to generate g-convex sets in $\mathcal{Q}_{\text{VALID}} \cap \mathcal{Q}_{\text{FREE}}$, and how to encode (6c). For $q = (\theta_{\text{L}}, \psi_{\text{R}})$ (or $q = (\theta_{\text{L}}, \psi_{\text{R}}, \mathcal{T})$ if the end effector transformation is allowed to vary), consider the auxiliary variable θ_{R} denoting the joint angles of the subordinate arm, computed with $(\theta_{\text{L}}, \theta_{\text{R}}) = \xi(q)$.

First, we require that any inverse trigonometric functions used in the analytic IK mapping $g_{i,j,\text{R}}$ do not violate their domains. Although this constraint would be enforced by the later constraints, specifically handling this case first greatly improves the performance of the later counterexample searches. For example, [34, Eq. 4] takes the arccos of an argument w , so we encode (6c) as $|w| \geq 1 + \epsilon$. When using the analytic IK solution for the KUKA iiwa, we enforce this constraint for equations (4), (6), (18), and (23) of [34].

Next, we check the joint limits (3b), encoded for (6c) as

$$\max(\xi(q) - \theta_{\text{max}}, \theta_{\text{min}} - \xi(q)) \geq \epsilon.$$

For reachability counterexamples (3a), we compute the squared Frobenius norm of the difference between desired

and realized end-effector pose, encoding (6c) as

$$\|\phi_{\mathcal{T}}(f_{\mathbf{L}}(\theta_{\mathbf{L}})) - f_{\mathbf{R}}(\theta_{\mathbf{R}})\|_F^2 \geq \epsilon.$$

These three constraints will ensure $\mathcal{H}(A, b) \subseteq \mathcal{Q}_{\text{VALID}}$. To also enforce $\mathcal{H}(A, b) \subseteq \mathcal{Q}_{\text{FREE}}$, we search for configurations q such that the robot is in collision. We separately find counterexamples for each pair of collision bodies, using equation (2) of [49]. Note that this equation operates on the full configuration $(\theta_{\mathbf{L}}, \theta_{\mathbf{R}})$, as obtained from the parametrized configuration with ξ . Because (6) is a nonlinear program, we solve it using SNOPT [58] with random initializations until a solution is obtained or a predefined number of consecutive failures is reached (and in that case, return infeasible).

IV. RESULTS

We demonstrate our new constrained planning framework using a bimanual manipulation setup with two *KUKA iiwa 7DoF* arms. Interactive recordings of all trajectories are available online at <https://cohnt.github.io/Bimanual-Web/>. We compute the analytic IK maps according to the methodology presented in [34]. To evaluate the merits of our IK parametrization for constrained planning, we consider a task where the two arms must move an object around a set of shelves, while avoiding collisions. We test four approaches under our parametrization:

- 1a. *IK-BiRRT*. We use the single-query bidirectional RRT (BiRRT) algorithm [39].
- 2a. *IK-Trajopt*. We directly solve (5) with kinematic trajectory optimization [59, §10.3], using the Drake modeling toolbox [60]. We use the output of the BiRRT planner as the initial guess for the trajectory optimizer.
- 3a. *IK-PRM*. We use the multi-query PRM algorithm [38], initialized with nodes from multiple BiRRTs to ensure connectivity, as in [5, §C].
- 4a. *IK-GCS*. We use GCS-planner [5] with 19 regions, constructed from hand-selected seed points.

For both the BiRRT and PRM plans, we use short-cutting to post-process the paths [61]. We solved the GCS problems with Mosek [62]. We compare these parametrized planners with constrained planning baselines.

- 1b. *Constrained Trajectory Optimization*. We solve (4) with kinematic trajectory optimization, using the IK-BiRRT plan as the initial guess to compare with IK-Trajopt.
- 2b. *Sampling-Based Planning*. For sampling-based planners, we use the single-query Atlas-BiRRT and multi-query Atlas-PRM algorithms [12], as implemented in the Open Motion Planning Library [63]. The atlas and PRM are initialized from multiple Atlas-BiRRT runs.

We do not compare to any GCS baseline without IK, as the constraint manifold is inherently nonconvex; IK-GCS is the first proposal for extending GCS to this class of problems.

Constraint Violations: Because the baseline methods can only enforce the kinematic constraint at discrete points, the constraint violation can be significant between such points. The OMPL planners experienced a maximum constraint violation of 6.76 cm, and the trajectory optimization baseline experienced a maximum constraint violation of 7.00

Method	Top to Middle	Middle to Bottom	Bottom to Top
Trajopt	4.24*	2.66*	6.10*
Atlas-BiRRT	5.57	5.60	6.76
Atlas-PRM	7.24	7.09	8.56
IK-Trajopt	2.64	3.00	4.75
IK-BiRRT	9.19	10.63	18.36
IK-PRM	4.13	13.75	13.65
IK-GCS	2.09	3.32	5.62

TABLE I: Path lengths (measured in configuration space) for each method with various start and goal configurations. Paths marked with an asterisk were not collision-free.

Method	Top to Middle	Middle to Bottom	Bottom to Top
Trajopt	43.78	48.03	61.50
Atlas-BiRRT	118.66	253.34	421.30
Atlas-PRM	7.54	14.71	17.28
IK-Trajopt	63.92	94.92	109.84
IK-BiRRT	57.10	70.50	97.08
IK-PRM	31.38	45.88	32.36
IK-GCS	3.41	2.32	3.32

TABLE II: Online planning time (in seconds) for each method with various start and goal configurations. Atlas-BiRRT runtimes were only averaged over successful runs (not including timeouts).

cm. In comparison, our parametrization methods maintained all constraints within 0.001 cm. Plans from the trajectory optimization baseline also collided with obstacles.

Path Length & Planning Time: Across all methods, for various start and goal configurations, we compare path length in Table I and online planning time in Table II. We ran both BiRRT methods 10 times for each plan, and report the average path length and planning time. We set a maximum planning time of 10 minutes for Atlas-BiRRT, and omit these from the averaging. Out of the 30 runs used for the table, Atlas-BiRRT timed out 22 times. IK-BiRRT never timed out; the longest plan took 319.12 seconds to compute. In Figure 4, we visualize several plans produced by the various constrained planning algorithms.

Table II does not include offline compute time. The time to construct the Atlas-PRM varies greatly; with three random seeds, it took 326.30, 1878.30, and 5405.54 seconds. Constructing the IK-PRM took 12124.21 seconds, and constructing the IRIS regions for GCS took 18361.36 seconds (966.39 seconds per region on average). The IRIS region construction can also be parallelized, improving runtime.

Overall, GCS is consistently able to achieve the fastest online runtimes, as a result of the offline precomputation of IRIS regions. IK-Trajopt is sometimes able to find shorter paths than GCS, since it has fewer constraints, but it can get stuck in local minima (see Figure 4). Although the atlas methodologies may find shorter paths than their IK counterparts, this is at the cost of significantly higher runtimes and potentially large kinematic constraint violations.

Task Space Coverage of IRIS Regions. In Figure 5, we superimpose the end-effector poses from many sampled bimanual configurations within individual IRIS regions. Despite the complicated nonlinear mapping, these convex sets

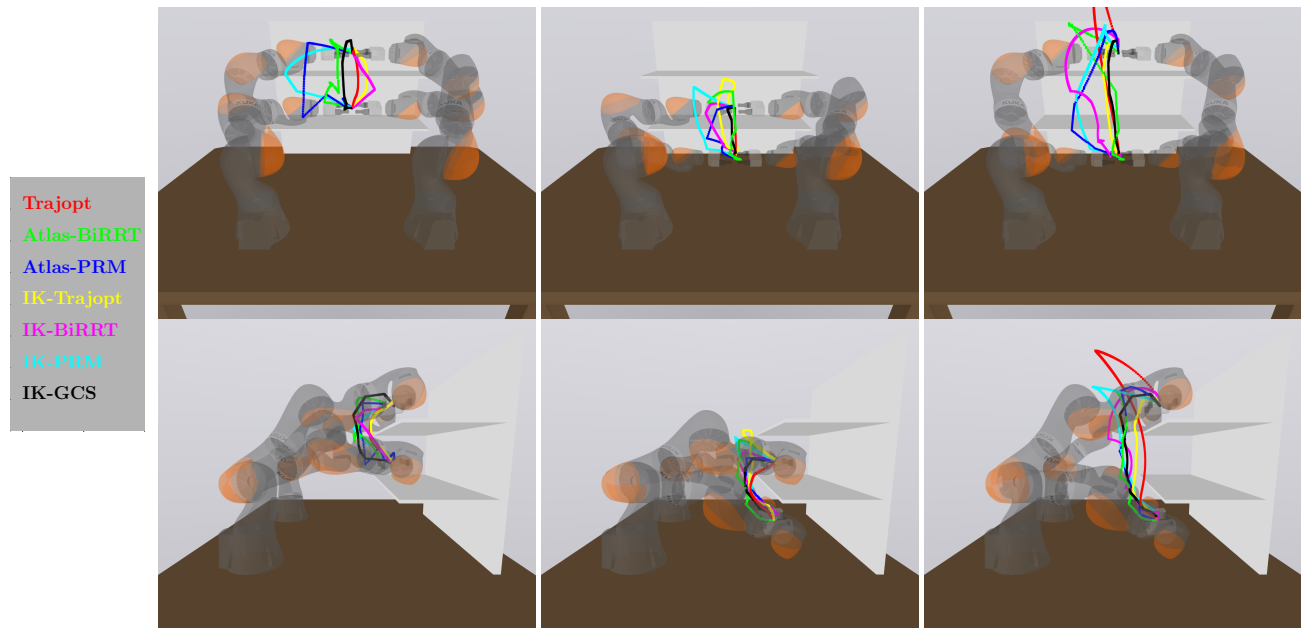
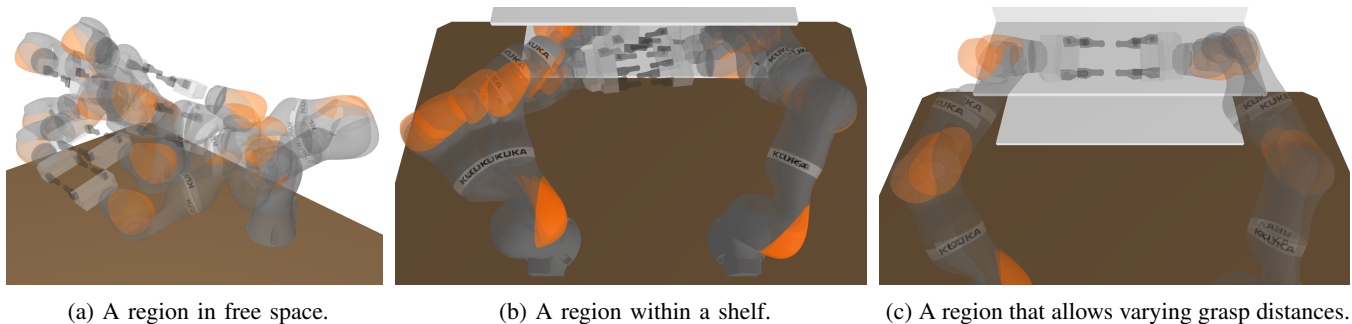


Fig. 4: Planned trajectories for reaching into shelves. The paths denote the end effector’s motion, and are colored by method.



(a) A region in free space.

(b) A region within a shelf.

(c) A region that allows varying grasp distances.

Fig. 5: Robot configurations sampled from various IRIS regions.

are able to cover large swaths of task space, as shown in Figure 5 (a). In Figure 5 (b), we demonstrate that IRIS regions can reliably encompass the motions required to reach into and out of a shelf. And in Figure 5 (c), we visualize an IRIS region that allows the grasp distance to vary. GCS can use such regions to plan motions for objects of different; we include hardware demonstrations in our results video.

V. DISCUSSION

We presented a novel parametrization of the constrained configuration space that arises in bimanual manipulation, which can be leveraged by both sampling-based planners and trajectory optimizers for more efficient planning. Our parametrization can be used to find shorter paths more quickly than existing approaches, and these paths will satisfy the kinematic constraints at all points along the trajectory. This parametrization also enables the use of planners such as GCS, which previously could not be applied to configuration spaces with nonlinear equality constraints.

Our parametrization is inherently asymmetric. Other choices of parametrization may seem more natural, such as:

- 1) Treating the end-effector configuration and redundancy parameters for both arms as the free variables, and using analytic IK for both arms.
- 2) Treating the first four joints of each arm as free variables, and solving IK for the remaining six joints as a virtual 6DoF arm whose middle link is represented by the object held by both end-effectors.

For the first option, we would have to choose global configuration parameters for both arms; in the case of the KUKA iiwa, this involves 64 choices (instead of the 8 options for our parametrization). Also, the shortest paths for the end effector may lead to very inefficient paths in joint space. (Our parametrization can at least minimize the work for one of the arms.) Finally, it requires planning over $SO(3)$, which cannot be used in with GCS (see [56, Thm. 5]).

For the second option, the choice of end-effector transformation \mathcal{T} determines the kinematic structure of the virtual arm, so different grasps would require different analytic IK solutions. Constructing such solutions would be time-consuming, and they may not always exist.

REFERENCES

- [1] D. Berenson, S. S. Srinivasa, D. Ferguson, and J. J. Kuffner, "Manipulation planning on constraint manifolds," in *2009 IEEE international conference on robotics and automation*. IEEE, 2009, pp. 625–632.
- [2] B. Krauskopf, H. M. Osinga, and J. Galán-Vioque, *Numerical continuation methods for dynamical systems*. Springer, 2007, vol. 2.
- [3] M. Bonilla, E. Farnioli, L. Pallottino, and A. Bicchi, "Sample-based motion planning for soft robot manipulators under task constraints," in *2015 IEEE International Conference on Robotics and Automation (ICRA)*. IEEE, 2015, pp. 2522–2527.
- [4] R. Bonalli, A. Cauligi, A. Bylard, T. Lew, and M. Pavone, "Trajectory optimization on manifolds: A theoretically-guaranteed embedded sequential convex programming approach," in *Proceedings of Robotics: Science and Systems*, Freiburg/Breisgau, Germany, June 2019.
- [5] T. Marcucci, M. Petersen, D. von Wrangel, and R. Tedrake, "Motion Planning around Obstacles with Convex Optimization," *arXiv preprint arXiv:2205.04422*, 2022.
- [6] M. Bonilla, L. Pallottino, and A. Bicchi, "Noninteracting constrained motion planning and control for robot manipulators," in *2017 IEEE International Conference on Robotics and Automation (ICRA)*. IEEE, 2017, pp. 4038–4043.
- [7] M. Stilman, "Global manipulation planning in robot joint space with task constraints," *IEEE Transactions on Robotics*, vol. 26, no. 3, pp. 576–584, 2010.
- [8] J. Mirabel, S. Tonneau, P. Fernbach, A.-K. Seppälä, M. Campana, N. Mansard, and F. Lamiroux, "Hpp: A new software for constrained motion planning," in *2016 IEEE/RSJ International Conference on Intelligent Robots and Systems (IROS)*. IEEE, 2016, pp. 383–389.
- [9] L. Jaillet and J. M. Porta, "Path planning under kinematic constraints by rapidly exploring manifolds," *IEEE Transactions on Robotics*, vol. 29, no. 1, pp. 105–117, 2012.
- [10] O. Bohigas, M. E. Henderson, L. Ros, M. Manubens, and J. M. Porta, "Planning singularity-free paths on closed-chain manipulators," *IEEE Transactions on Robotics*, vol. 29, no. 4, pp. 888–898, 2013.
- [11] B. Kim, T. T. Um, C. Suh, and F. C. Park, "Tangent bundle rrt: A randomized algorithm for constrained motion planning," *Robotica*, vol. 34, no. 1, pp. 202–225, 2016.
- [12] Z. Kingston, M. Moll, and L. E. Kavraki, "Exploring implicit spaces for constrained sampling-based planning," *The International Journal of Robotics Research*, vol. 38, no. 10-11, pp. 1151–1178, 2019.
- [13] L. Han, L. Rudolph, J. Blumenthal, and I. Valodzin, "Convexly stratified deformation spaces and efficient path planning for planar closed chains with revolute joints," *The International Journal of Robotics Research*, vol. 27, no. 11-12, pp. 1189–1212, 2008.
- [14] T. McMahon, S. Thomas, and N. M. Amato, "Sampling-based motion planning with reachable volumes for high-degree-of-freedom manipulators," *The International Journal of Robotics Research*, vol. 37, no. 7, pp. 779–817, 2018.
- [15] F. Zha, Y. Liu, W. Guo, P. Wang, M. Li, X. Wang, and J. Li, "Learning the metric of task constraint manifolds for constrained motion planning," *Electronics*, vol. 7, no. 12, p. 395, 2018.
- [16] I. A. Şucan and S. Chitta, "Motion planning with constraints using configuration space approximations," in *2012 IEEE/RSJ International Conference on Intelligent Robots and Systems*. IEEE, 2012, pp. 1904–1910.
- [17] Z. Kingston, M. Moll, and L. E. Kavraki, "Sampling-based methods for motion planning with constraints," *Annual review of control, robotics, and autonomous systems*, vol. 1, pp. 159–185, 2018.
- [18] F. Kanehiro, E. Yoshida, and K. Yokoi, "Efficient reaching motion planning and execution for exploration by humanoid robots," in *2012 IEEE/RSJ International Conference on Intelligent Robots and Systems*. IEEE, 2012, pp. 1911–1916.
- [19] D. Rakita, B. Mutlu, and M. Gleicher, "Relaxedik: Real-time synthesis of accurate and feasible robot arm motion," in *Robotics: Science and Systems*, vol. 14. Pittsburgh, PA, 2018, pp. 26–30.
- [20] F. Burget, A. Hornung, and M. Bennewitz, "Whole-body motion planning for manipulation of articulated objects," in *2013 IEEE International Conference on Robotics and Automation*. IEEE, 2013, pp. 1656–1662.
- [21] B. Siciliano, O. Khatib, and T. Kröger, *Springer handbook of robotics*. Springer, 2008, vol. 200.
- [22] R. Tedrake, *Robotic Manipulation*, 2023. [Online]. Available: <http://manipulation.mit.edu>
- [23] M. Raghavan and B. Roth, "Inverse kinematics of the general 6r manipulator and related linkages," *Journal of Mechanical Design*, vol. 115, no. 3, pp. 502–508, sep 1993. [Online]. Available: <https://doi.org/10.1115/1.2919218>
- [24] J. Nielsen and B. Roth, "On the kinematic analysis of robotic mechanisms," *The International Journal of Robotics Research*, vol. 18, no. 12, pp. 1147–1160, 1999.
- [25] S. Xie, L. Sun, G. Chen, Z. Wang, and Z. Wang, "A novel solution to the inverse kinematics problem of general 7r robots," *IEEE Access*, vol. 10, pp. 67 451–67 469, 2022.
- [26] B. Siciliano, L. Sciavicco, L. Villani, and G. Oriolo, *Robotics*. Springer London, 2009.
- [27] R. Diankov, "Automated construction of robotic manipulation programs," Ph.D. dissertation, Carnegie Mellon University, The Robotics Institute Pittsburgh, 2010.
- [28] R. Diankov and J. Kuffner, "Openrave: A planning architecture for autonomous robotics," *Robotics Institute, Pittsburgh, PA, Tech. Rep. CMU-RI-TR-08-34*, vol. 79, 2008.
- [29] K. P. Hawkins, "Analytic inverse kinematics for the universal robots ur-5/ur-10 arms," *Georgia Institute of Technology, Tech. Rep.*, 2013.
- [30] K. Hauser, "Continuous pseudoinversion of a multivariate function: Application to global redundancy resolution," in *Algorithmic Foundations of Robotics XII: Proceedings of the Twelfth Workshop on the Algorithmic Foundations of Robotics*. Springer, 2020, pp. 496–511.
- [31] A. Hemami, "A more general closed-form solution to the inverse kinematics of mechanical arms," *Advanced robotics*, vol. 2, no. 4, pp. 315–325, 1987.
- [32] J. M. Hollerbach, "Optimum kinematic design for a seven degree of freedom manipulator," in *Robotics research: The second international symposium*. Citeseer, 1985, pp. 215–222.
- [33] M. Shimizu, H. Kakuya, W.-K. Yoon, K. Kitagaki, and K. Kosuge, "Analytical inverse kinematic computation for 7-dof redundant manipulators with joint limits and its application to redundancy resolution," *IEEE Transactions on robotics*, vol. 24, no. 5, pp. 1131–1142, 2008.
- [34] C. Faria, F. Ferreira, W. Erlhagen, S. Monteiro, and E. Bicho, "Position-based kinematics for 7-dof serial manipulators with global configuration control, joint limit and singularity avoidance," *Mechanism and Machine Theory*, vol. 121, pp. 317–334, 2018.
- [35] Y. He and S. Liu, "Analytical inverse kinematics for franka emika panda—a geometrical solver for 7-dof manipulators with unconventional design," in *2021 9th International Conference on Control, Mechatronics and Automation (ICCM)*. IEEE, 2021, pp. 194–199.
- [36] G. K. Singh and J. Claassens, "An analytical solution for the inverse kinematics of a redundant 7dof manipulator with link offsets," in *2010 IEEE/RSJ International Conference on Intelligent Robots and Systems*. IEEE, 2010, pp. 2976–2982.
- [37] S. M. LaValle *et al.*, "Rapidly-exploring random trees: A new tool for path planning," 1998.
- [38] L. E. Kavraki, P. Svestka, J.-C. Latombe, and M. H. Overmars, "Probabilistic roadmaps for path planning in high-dimensional configuration spaces," *IEEE transactions on Robotics and Automation*, vol. 12, no. 4, pp. 566–580, 1996.
- [39] J. J. Kuffner and S. M. LaValle, "Rrt-connect: An efficient approach to single-query path planning," in *Proceedings 2000 ICRA. Millennium Conference. IEEE International Conference on Robotics and Automation. Symposia Proceedings (Cat. No. 00CH37065)*, vol. 2. IEEE, 2000, pp. 995–1001.
- [40] R. Bohlin and L. E. Kavraki, "Path planning using lazy prm," in *Proceedings 2000 ICRA. Millennium conference. IEEE international conference on robotics and automation. Symposia proceedings (Cat. No. 00CH37065)*, vol. 1. IEEE, 2000, pp. 521–528.
- [41] L. Jaillet, J. Cortés, and T. Siméon, "Sampling-based path planning on configuration-space costmaps," *IEEE Transactions on Robotics*, vol. 26, no. 4, pp. 635–646, 2010.
- [42] S. Karaman and E. Frazzoli, "Sampling-based algorithms for optimal motion planning," *The international journal of robotics research*, vol. 30, no. 7, pp. 846–894, 2011.
- [43] I. Ko, B. Kim, and F. C. Park, "Randomized path planning on vector fields," *The International Journal of Robotics Research*, vol. 33, no. 13, pp. 1664–1682, 2014.
- [44] O. Salzman and D. Halperin, "Asymptotically near-optimal rrt for fast, high-quality motion planning," *IEEE Transactions on Robotics*, vol. 32, no. 3, pp. 473–483, 2016.
- [45] M. Otte and E. Frazzoli, "Rrtx: Asymptotically optimal single-query sampling-based motion planning with quick replanning," *The Inter-*

- national Journal of Robotics Research*, vol. 35, no. 7, pp. 797–822, 2016.
- [46] M. Zucker, N. Ratliff, A. D. Dragan, M. Pivtoraiko, M. Klingensmith, C. M. Dellin, J. A. Bagnell, and S. S. Srinivasa, “Chomp: Covariant hamiltonian optimization for motion planning,” *The International Journal of Robotics Research*, vol. 32, no. 9–10, pp. 1164–1193, 2013.
- [47] M. Kalakrishnan, S. Chitta, E. Theodorou, P. Pastor, and S. Schaal, “STOMP: Stochastic trajectory optimization for motion planning,” in *2011 IEEE international conference on robotics and automation*. IEEE, 2011, pp. 4569–4574.
- [48] M. Toussaint, “A tutorial on newton methods for constrained trajectory optimization and relations to slam, gaussian process smoothing, optimal control, and probabilistic inference,” *Geometric and numerical foundations of movements*, pp. 361–392, 2017.
- [49] M. Petersen and R. Tedrake, “Growing convex collision-free regions in configuration space using nonlinear programming,” *arXiv preprint arXiv:2303.14737*, 2023.
- [50] T. Marcucci, P. Nobel, R. Tedrake, and S. Boyd, “Fast path planning through large collections of safe boxes,” *arXiv preprint arXiv:2305.01072*, 2023.
- [51] E. Fernández González *et al.*, “Generative multi-robot task and motion planning over long horizons,” Ph.D. dissertation, Massachusetts Institute of Technology, 2018.
- [52] R. Deits and R. Tedrake, “Efficient mixed-integer planning for uavs in cluttered environments,” in *2015 IEEE international conference on robotics and automation (ICRA)*. IEEE, 2015, pp. 42–49.
- [53] D. H. Gottlieb, “Topology and the robot arm,” *Acta Applicandae Mathematica*, vol. 11, pp. 117–121, 1988.
- [54] J. W. Burdick, “On the inverse kinematics of redundant manipulators: Characterization of the self-motion manifolds,” in *Advanced Robotics: 1989: Proceedings of the 4th International Conference on Advanced Robotics Columbus, Ohio, June 13–15, 1989*. Springer, 1989, pp. 25–34.
- [55] C. L. Luck and S. Lee, “Self-motion topology for redundant manipulators with joint limits,” in *[1993] Proceedings IEEE International Conference on Robotics and Automation*. IEEE, 1993, pp. 626–631.
- [56] T. Cohn, M. Petersen, M. Simchowitz, and R. Tedrake, “Non-Euclidean Motion Planning with Graphs of Geodesically-Convex Sets,” in *Proceedings of Robotics: Science and Systems*, Daegu, Republic of Korea, July 2023.
- [57] J. M. Lee and J. M. Lee, *Smooth manifolds*. Springer, 2012.
- [58] P. E. Gill, W. Murray, and M. A. Saunders, “SNOPT: An SQP algorithm for large-scale constrained optimization,” *SIAM Rev.*, vol. 47, pp. 99–131, 2005.
- [59] R. Tedrake, *Underactuated Robotics*, 2023. [Online]. Available: <https://underactuated.csail.mit.edu>
- [60] R. Tedrake and the Drake Development Team, “Drake: Model-based design and verification for robotics,” 2019. [Online]. Available: <https://drake.mit.edu>
- [61] F. Schwarzzer, M. Saha, and J.-C. Latombe, “Exact collision checking of robot paths,” *Algorithmic foundations of robotics V*, pp. 25–41, 2004.
- [62] M. ApS, “MOSEK Optimization Suite,” 2019.
- [63] I. A. Şucan, M. Moll, and L. E. Kavraki, “The Open Motion Planning Library,” *IEEE Robotics & Automation Magazine*, vol. 19, no. 4, pp. 72–82, December 2012, <https://ompl.kavrakilab.org>.